Available online at www.sciencedirect.com
ScienceDirect
Journal of the European Ceramic Society 28 (2008) 2049–2055
www.elsevier.com/locate/jeurceramsoc

Piezospectroscopic measurement of the stress field around an indentation crack tip in ruby using SEM cathodoluminescence

R.I. Todd [a,*], D. Stowe [a,b], S. Galloway [b], D. Barnes [a], P.R. Wilshaw [a]

[a] *University of Oxford, Department of Materials, Parks Road, Oxford OX1 3PH, UK*
[b] *Gatan UK, 25 Nuffield Way, Abingdon, Oxon OX14 1RL, UK*

Received 12 August 2007; received in revised form 31 January 2008; accepted 1 February 2008
Available online 8 April 2008

Abstract

Piezospectroscopy using stress-sensitive lines in the cathodoluminescence (CL) spectrum generated in response to excitation by the electron beam of an SEM has recently been shown to be a promising technique for submicron resolution stress measurements in alumina and other ceramics. This paper develops and applies the technique by mapping the wavelength shifts of the R_1 CL line around the tip of an indentation crack in a ruby single crystal. Accounting for crystallographic anisotropy, the shifts observed were quantitatively consistent with the classical crack tip stress field for all polar angles ahead of the crack tip and indicated a crack tip stress intensity factor of 1.0 MPa $m^{1/2}$. This is significantly lower than the fracture toughness of the crack plane (4.5 MPa $m^{1/2}$), and indicates the post-indentation development of lateral cracks and slow crack growth. The spatial resolution of the stress measurements was measured as 550 nm and the effects of specimen heating by the electron beam were shown to be negligible.

Keywords: Spectroscopy; Fracture; Toughness and Toughening; Al_2O_3; Cathodoluminescence

1. Introduction

Ceramic components often contain residual stresses. These have many sources, including plastic deformation due to indentation or abrasion, phase transformations and thermal expansion mismatches. The residual stresses may be beneficial or detrimental to the mechanical properties. Either way, it is important for the stresses to be investigated and understood.

This task is made difficult by the fine scale of many sources of stress and the lack of measurement techniques with sufficiently high spatial resolution that are suitable for bulk specimens. One technique that has been applied successfully to a wide range of ceramics and glasses is optical microprobe piezospectroscopy (OMPS).[1,2] In this technique a laser is focused to a small spot through the objective lens of an optical microscope. Any photoluminescence produced in response to this excitation is collected by the same lens and analysed using a spectrometer. Lines in the luminescence spectrum can be produced by several phenomena and their wavelength is often sensitive to stress. By suitable calibration this method can therefore be used for the measurement of the stresses within the sampling volume.

The spatial resolution of OMPS is restricted to ~2 μm by the diffraction-limited optics of the microscope used. Clearly, this could be improved if either the luminescence generation volume or the collection volume were released from this constraint. A practical way of achieving this is to retain the diffraction-limited collection optics, but to excite cathodoluminescence (CL) using the potentially much smaller generation volume of a focused electron beam in an SEM.

SEM-CL is widely used to investigate the properties of semiconductors and related materials and there are many reports of the sensitivity of CL wavelength to stress in such studies (e.g. see Refs. [3,4]). In many cases this is peripheral to the aims of the investigation but Rudloff et al.[5] have presented a detailed investigation of the stresses in microcracked $Al_xGa_{1-x}N$ films. Maps of the stress-induced shift in luminescence wavelength were obtained using computer control of the SEM electron beam and compared favourably with the predictions of a FE model for the films.

* Corresponding author. Fax: +44 1865 273783.
E-mail address: richard.todd@materials.ox.ac.uk (R.I. Todd).

0955-2219/$ – see front matter © 2008 Elsevier Ltd. All rights reserved.
doi:10.1016/j.jeurceramsoc.2008.02.008

It is also possible to make SEM-CL stress measurements on metal oxides. Pezzotti et al. have reported SEM-CL stress measurements from several glass compositions [6] with accelerating voltages as low as 1 kV, which leads to a potentially very small luminescence generation volume and correspondingly improved spatial resolution. Stress maps based on measured wavelength shifts near imperfections in clad optical fibres are presented.

The ability to make high resolution stress measurements on the surface of bulk specimens of structural ceramics, such as alumina, would be very useful. The first systematic attempt to measure stresses in alumina using SEM-CL was by Ostertag et al. in 1991[7] who measured the stresses around a hardness indentation in a single crystal using the shift in the luminescence associated with Cr impurities, the so-called ruby R_1 and R_2 lines. The accelerating voltage used was 20 kV resulting in a spatial resolution of around 5 μm, i.e. slightly worse than the OMPS technique described above. A further problem was in obtaining sufficient signal, and noise in the spectrum led to considerable uncertainty in the stress measurements. Despite these limitations, systematic variations in stress around the indentations were convincingly observed.

Recently, Pezzotti et al.[8] have shown that the ruby R_1 and R_2 lines can be collected using the lower accelerating voltages required for high spatial resolution measurements. The R line wavelength shifts directly ahead of an indentation crack were measured and used in conjunction with the crack tip stress intensity, measured independently, to estimate the relationship between the line shift and stress. A hydrostatic stress map around the indentation is presented based on this calibration.

The work of Pezzotti et al.[8] is encouraging, but raises several issues needing clarification. Firstly, the plot of R_1 line shift against $1/\sqrt{r}$ presented, where r is distance ahead of the crack tip, does not extrapolate to the origin and therefore does not have the simple proportionality expected from the classical crack tip stress field. Secondly, the stress mapping should be seen as semi-quantitative, both because of the above uncertainty over the form of the stress field used in the calibration and because this calibration procedure does not account for the considerable crystallographic anisotropy of the piezospectroscopic coefficients[9]. Finally, the resolution of the technique is not measured, although the wavelength variation behind the crack tip in the plot of line shift against r presented suggests a resolution ~1 μm.

This paper investigates these issues by mapping the stress-induced shifts of the R lines in the CL spectrum around the tip of an indentation crack in single crystal ruby taking into account the piezospectroscopic anisotropy of the crystal. This provides a comprehensive comparison between the line shifts and the classical stress field in all directions from the crack tip, not just the straight ahead direction. The crack tip singularity provides a convenient method of quantifying the resolution of the experimental technique as used in the present work.

2. Experimental

All measurements were carried out on a 0.5 mm thick $\{1\,1\,\bar{2}\,0\}$ (a-plane) slice of a ruby single crystal containing 0.05–0.1% Cr (Rubicon Technology, IL, USA, manufacturer's data for Cr content). One surface of the crystal was polished using 0.25 μm diamond paste and then annealed in air for 1 h at 1 550 °C to remove surface residual stresses. Vickers hardness indentations were made on the surface of the ruby using a load of 1 kg. The indentations were orientated so that the diagonals were parallel to the m and c axes of the crystal. The indented specimen spent approximately 20 h stored under vacuum and 2 h open to the atmosphere prior to CL spectra being taken.

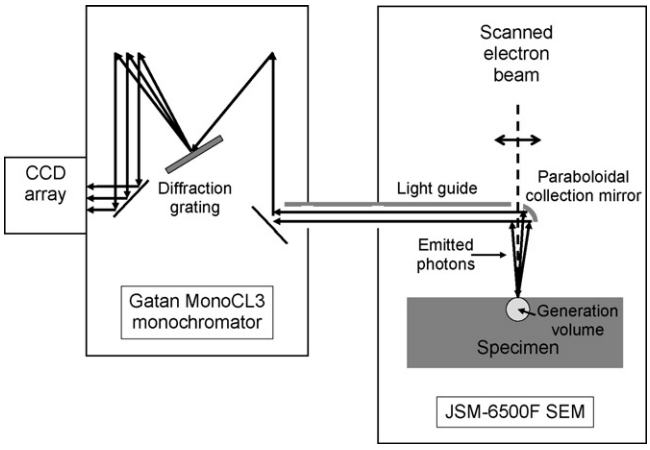

Fig. 1. Schematic of the CL system showing light paths.

The specimen was coated with a layer of carbon to minimise charging. The coating was sufficiently thin to allow most of the CL emission to pass through. Indentation cracks were examined at room temperature in a JSM-6500F SEM equipped with a Gatan XiCL*one* system. The experimental setup is shown schematically in Fig. 1. The CL emissions in response to the electron beam are collected by a paraboloidal mirror which, in conjunction with a system of lenses and mirrors, transmits the light collected to a diffraction grating. The diffracted spectrum is collected directly using a Princeton Instruments Spec-10 CCD camera. The system includes digital beam control software which enables the automated collection of a spectrum for each pixel within a user-defined region of interest, thus creating a three-dimensional data set with spectral information as a function of position (spectrum imaging).

Maps of the CL spectrum were collected around indentation crack tips with an accelerating voltage of 10 kV and absorbed specimen currents of ~1 nA using a pixel size of 0.22 μm × 0.22 μm. Several crack tips were mapped in this way, but the detailed analysis presented here is confined to results from the tip of a well developed indentation radial crack on the basal plane of the ruby and intersecting the surface along the m-axis of the crystal.

Fig. 2 shows a typical R line doublet collected using this system. Only the stronger R_1 line was used in the present work and its wavelength was defined for each pixel by fitting a Gaussian profile to the central portion of the line.

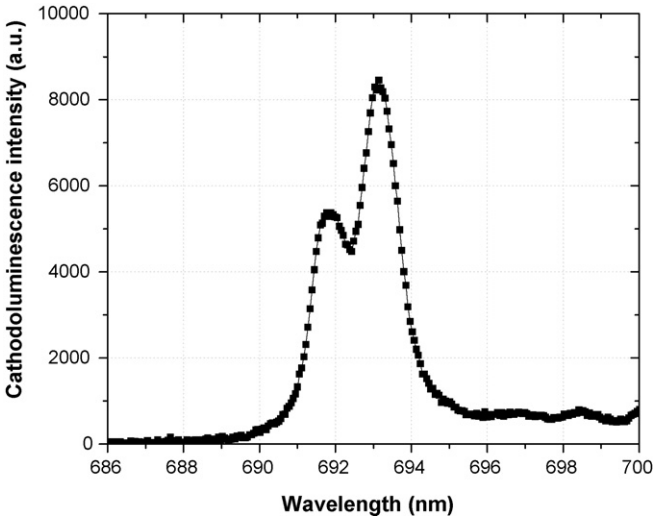

Fig. 2. Typical *R* line doublet collected using the system shown in Fig. 1.

3. Results and discussion

3.1. Raw results

Fig. 3 shows an optical micrograph of a typical 1 kg Vickers hardness indentation in the annealed ruby. Classical radial cracks emanate from three of the corners, but the "northern" indentation corner, is associated with a pair of radial cracks and several additional, smaller cracks can also be seen to have propagated from other parts of the indentation. Substantial subsurface lateral cracking is also evident, particularly in the "north western" quadrant. The dimensions of the indentation give a hardness of 1.6 GPa.

Fig. 4 shows a contour plot of the wavelength of the R_1 CL peak in the vicinity of the tip of a well developed indentation radial crack on the basal plane of the ruby, intersecting the surface along the crystal *m*-axis. The arrow on the base of the plot indicates the direction of crack propagation and terminates at the approximate position of the crack tip. It is clear that the R_1 wavelength is significantly reduced near the crack tip, indicating a strongly tensile stress field relative to the surroundings. It is reasonable to suppose that this arises from Mode I loading of the crack by the residual stress field of the indentation. The following section tests this possibility quantitatively.

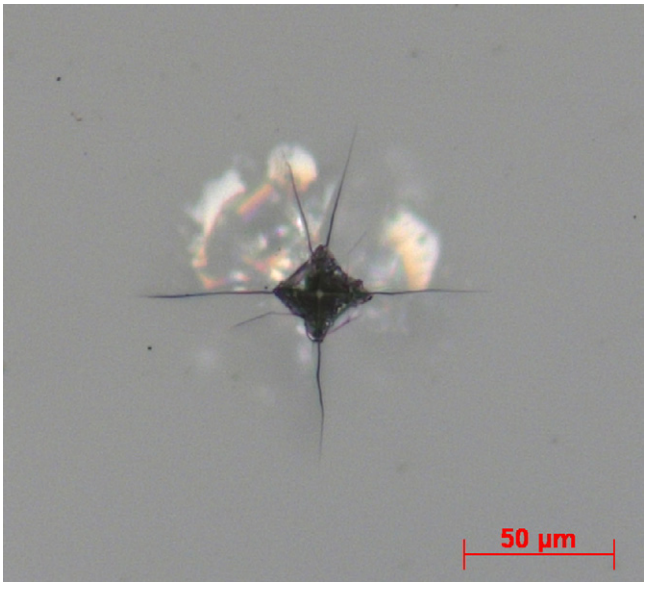

Fig. 3. 1 kg Vickers hardness indentation in polished and annealed ruby, showing radial and lateral cracking.

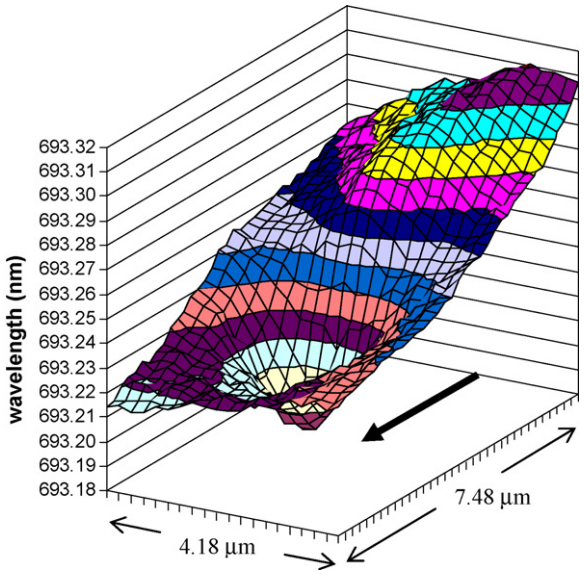

Fig. 4. Contour plot of the wavelength of the R_1 CL peak in the vicinity of the crack tip. Tick marks on the positional axes denote 0.22 µm pixels and the bold arrow shows the approximate trace of the crack.

3.2. Comparison of results with theoretical crack tip stress field

The theoretical Mode I crack tip stress field can be used in conjunction with values for the piezospectroscopic coefficients to predict the peak shifts in Fig. 4. The effect of the mild elastic anisotropy of ruby on the stress field was assessed using the analysis of Sih et al.[10]. Using the sapphire elastic constants of Wachtman et al.[11], it was found that the hydrostatic stress component predicted was within 8% of the elastically isotropic solution for all points, and within 4% for points ahead of the crack tip (i.e. absolute value of the polar angle θ, defined below, <90°). The low chromium content of our ruby (<0.1%) is unlikely to modify this conclusion significantly. For simplicity, therefore, we compare our results with the more familiar elastically isotropic crack tip stress field.

Combining the Mode I crack tip stress field for plane stress with the appropriate piezospectroscopic coefficients shows that the peak shift, $\Delta\lambda$, near a crack with the present crystallographic orientation is given by:

$$\Delta\lambda = -\lambda^2\Delta\nu = -\lambda^2 \cdot \frac{K}{\sqrt{2\pi r}}\left[\cos\frac{\theta}{2}\left(1-\sin\frac{\theta}{2}\sin\frac{3\theta}{2}\right)\Pi_m + \cos\frac{\theta}{2}\left(1+\sin\frac{\theta}{2}\sin\frac{3\theta}{2}\right)\Pi_c\right] \quad (1)$$

where λ is the stress-free wavelength of the R_1 peak, $\Delta\nu$ is the peak shift expressed in terms of wavenumber, K is the stress intensity factor, Π_m and Π_c are the wavenumber piezospectroscopic coefficients for the R_1 line for stresses parallel with the m and c axes, and r and θ are polar co-ordinates with the origin at the crack tip and the direction of crack propagation corresponding to $\theta = 0^\circ$.

The Mode I stress intensity factor, K, is unknown *a priori*, and quantitative comparison of Eq. (1) with the experimental results is complicated by the following factors:

(i) The precise position of the crack tip is difficult to determine because of the finite resolution of the technique; it should be noted that the position of lowest wavelength in Fig. 4 is expected to lie a short distance *beyond* the true crack tip because when the electron beam is centred on the tip itself, some of the nearly stress-free material immediately behind the crack tip is sampled by the interaction volume.

(ii) The stress field surrounding the plastic zone of the indentation is superimposed on the crack tip stress field in the case of indentation cracks. Optical microprobe measurements, also using the ruby R lines, around indentations in the same ruby[12] showed that the mean stress was compressive close to the indentation and became more positive with increasing distance from it.

(iii) The CL system exhibited a small apparent wavelength shift with electron beam position on the sample owing to geometrical effects in the optics. The shift was proportional to beam displacement[12] and with the crack orientation studied here was greatest for beam displacements parallel to the crack.

The approach taken was to fit Eq. (1) to the experimental results with K and the crack tip position as variables, and with the wavelength results corrected empirically for the combined effects of (ii) and (iii) above by subtracting a linear background with adjustable gradient sloping in the direction of crack propagation. Note that whilst the peak shift in (ii) did not vary linearly with distance in reality, the distance covered by the CL measurements was sufficiently small for it to be considered so[12].

Thus there are three adjustable parameters, all with clear physical interpretations and a narrow range of sensible values. The least squares fit was carried out with $\Pi_m = 3.50\,\mathrm{cm}^{-1}\,\mathrm{GPa}^{-1}$ and $\Pi_c = 1.53\,\mathrm{cm}^{-1}\,\mathrm{GPa}^{-1}$.[9] The position of the crack tip along the direction of propagation is included through the values of r and θ used to calculate the predicted peak shift for each pixel using Eq. (1). The fitting procedure described requires a reference wavelength from a point at which the wavelength shift from the crack tip stress field should be zero but which is sufficiently close to the crack tip for the linear approximation of the indentation stress field to remain valid. Eq. (1) shows that the crack tip stress field gives $\Delta\lambda = 0$ for $\theta = 180^\circ$ so the experimental value for λ at the point within the measured area which was on the crack and furthest from its tip was used as this reference. Only data from pixels with $r \geq 1\,\mu\mathrm{m}$ and $|\theta| < 90^\circ$ were used in the fitting. The former constraint was required to exclude points close to the crack tip where the resolution of the technique may have limited its accuracy (see Section 3.4) and the latter because the crack path was not sufficiently straight to allow points behind the crack tip to conform accurately to Eq. (1).

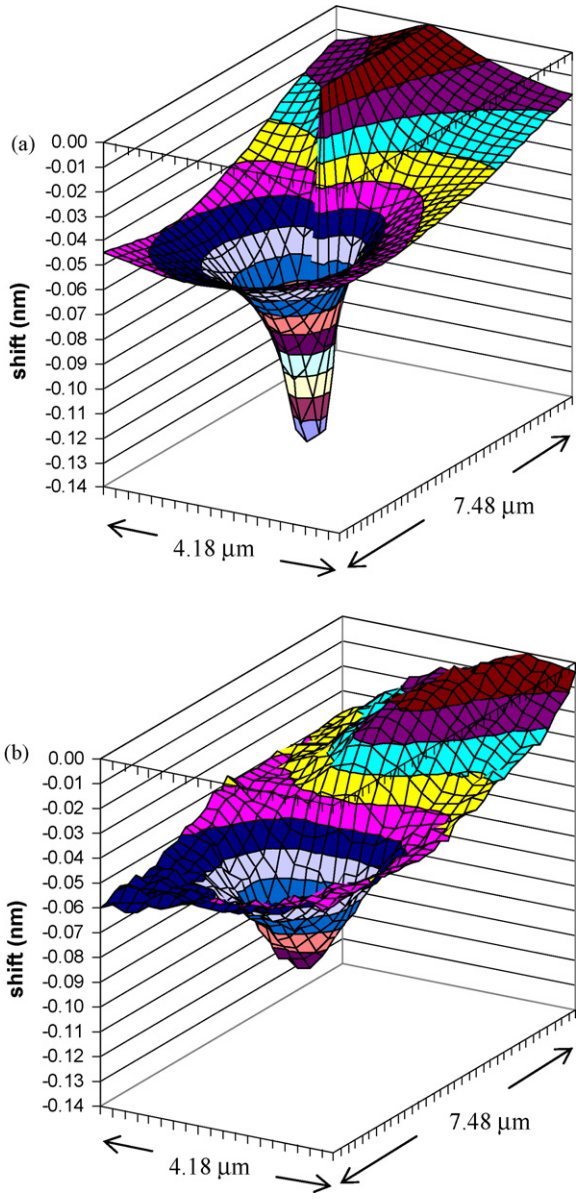

Fig. 5. (a) R_1 Peak shifts predicted from Eq. (1) using the best fit parameters, and (b) experimental peak shifts corrected for the effects of the indentation stress field and geometrical shift. Both plots have the same scales on the axes.

Fig. 5 compares the peak shifts predicted from Eq. (1), using the best fit parameters, with the experimental results, corrected for the effects of the indentation stress field and geometrical shift. Away from the crack tip, at which Eq. (1) predicts an infinite peak shift, the shifts are of similar order, and this is confirmed by Fig. 6, which shows the residual (i.e. experimental shift minus predicted shift). Except at the crack tip, the residual

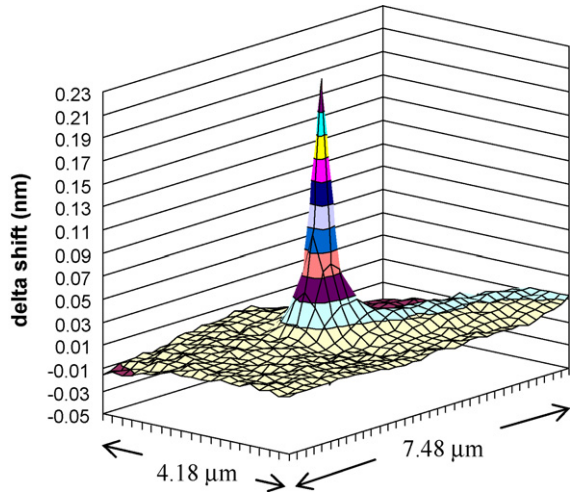

Fig. 6. The residual (i.e. experimental shift—predicted shift), for the data of Fig. 5.

is essentially zero ahead of the crack, demonstrating excellent agreement between the experimental results and the classical Mode I crack tip stress field. This is also demonstrated in Fig. 7, which compares theory and experimental data presented as plots of peak shift vs. $1/\sqrt{r}$ for $\theta = 0°$ and $\pm 90°$. The experimental points lie close to the straight lines through the origin predicted by Eq. (1) for these values of θ.

The fitted gradient of the background wavelength shift parallel to the crack, which was introduced to account for the indentation stress field and geometrical effects in the optics as described above, was 0.005 nm/µm. This is of the order of magnitude expected from the preliminary experiments[12] and is a relatively minor effect, whose contribution over the full length of the map is much less than the peak shifts seen in the vicinity of the crack tip. The fitted crack tip position was 0.78 µm behind the point of minimum wavelength and coincides with the mostly steeply rising part of the wavelength map along the crack path, as might have been a suitable estimate of the crack tip position without the fitting procedure. The only significantly adjustable parameter is therefore K. This demonstrates that the excellent agreement between theory and experiment in two dimensions

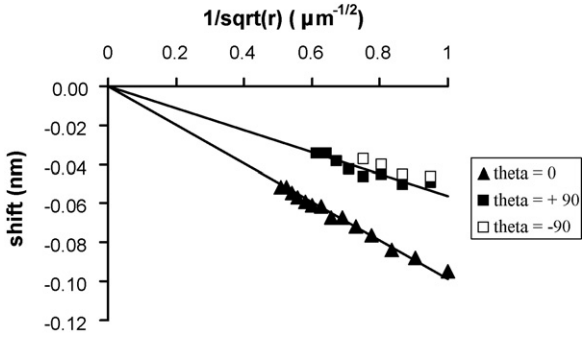

Fig. 7. R_1 peak shift vs. $1/\sqrt{r}$ for $\theta = 0°$ and $\pm 90°$ and $r \geq 1$ µm (the results are affected by the finite resolution of the technique for smaller values of r). Points are experimental and solid lines are the predictions of Eq. (1) for $K = 1.0$ MPa m$^{1/2}$ for the same values of θ.

shown in Figs. 5–7 is meaningful and is not simply the result of a curve fitting exercise.

3.3. Stress intensity factor and toughness values

The fitted value of the stress intensity factor, K, was 1.0 MPa m$^{1/2}$. This is much lower than the crack plane (0 0 0 1) toughness of sapphire measured by fast fracture of 4.5 MPa m$^{1/2}$.[13] This was true of all the cracks examined during our preliminary investigations; indeed the crack studied here was selected for further investigation because its crack tip stress field was more pronounced than most.

It seems unlikely that the small amount of chromium dopant can be responsible for such a big discrepancy. Moisture assisted slow growth of the radial cracks in the time between indentation and the CL study in the SEM provides a more plausible explanation, as crack growth rates in sapphire are relatively rapid down to stress intensities of around 1 MPa m$^{1/2}$.[14] A further possibility is that the subsurface lateral cracking evident in Fig. 3 may have unloaded the radial cracks after their formation; surface chipping due to growth of lateral cracks towards the surface was sometimes seen to occur many minutes after indentation.

The importance of lateral cracking is supported by comparing the above stress intensity value with the figure of 1.9 MPa m$^{1/2}$ estimated from the radial crack length and hardness using the formula of Anstis et al.[15]. If slow crack growth alone had been responsible for the low stress intensity in the present direct CL measurements it should have been reflected in the value deduced from the indentation crack length as well. The significant discrepancy highlighted suggests that lateral cracking reduced the central loading of the radial–median system by the indentation plastic zone after the formation of this crack system. This has serious implications for the analysis of indentation-strength toughness measurements[16] on very brittle materials such as sapphire, as this method assumes that the radial-median crack system remains fully loaded by the indentation plastic zone during final fracture.

3.4. Spatial resolution of CL measurements

The residual indicates a spatial resolution (estimated as the half width at the base of the residual peak in Fig. 6) of 550 nm. This value is not related to the arbitrary limit of $r = 1$ µm below which points were excluded from the fitting, as described in Section 3.2; the fitted parameters and residual are very insensitive to the distance within which points are excluded because of the large number of points further from the crack tip. The resolution is significantly better than can be achieved using photoluminescence in systems based on optical microscopes, which are limited to lateral resolutions of ~ 2 µm.

The electron spot size at the surface of the specimen is no more than a few nanometres under the conditions used so it is clear that this does not control the resolution. The resolution can be compared with the Grün range, as modified by

Everhart and Hoff[17]:

$$R_G = \frac{4.28 \times 10^{-6}}{\rho} E^{1.75}$$

in which R_G is in cm, the density, ρ is in g cm^{-3} and the accelerating voltage of the incident electrons, E, is in kV. R_G is a measure of the depth below the surface to which electron–hole pairs are generated, but since the interaction volume is roughly spherical, it has also been identified with the lateral resolution. With $\rho = 4$ g cm^{-3} and $E = 10$ kV, $R_G = 600$ nm, which is close to the resolution of our experiments. This comparison should be treated with caution, however. The distribution of energy dissipation within the generation volume is highly inhomogeneous, being very sharply peaked towards the centre of the volume indicating that the Grün range may in fact be a significantly pessimistic estimate of the ideal resolution. This suggests that other effects cause a degradation of the resolution. Some of these may be inherent to the specimen, such as saturation and carrier diffusion before recombination. In the present case, however, beam drift due to charging is also likely to have been a significant factor; drifts over the period of data collection (~30 min), measured by comparing secondary electron images taken before and after the measurements, were up to 200 nm.

3.5. Influence of specimen heating

One problem with increasing the resolution of piezospectroscopic measurements is that the amount of fluorescent light generated is rapidly reduced as the volume from which it comes gets smaller. It is possible to compensate for this to some extent by increasing the degree of excitation, in the case of CL by increasing the beam current. If the beam current is too high, however, specimen heating can cause errors in the stress measurements. This is both because there is a direct effect of a stress-free temperature on the wavelength of the R lines[9] and because local heating in a bulk specimen itself causes residual stresses. In a uniform sample these are simply superposed on the pre-existing stresses of interest, but near a surface, interface or second phase the heat flow will be perturbed and spurious stress variations will result.

We estimate the beam heating effect in our measurements by approximating the interaction volume between the incident electrons and the sample to a hemisphere of radius r_0 with planar surface coincident with the sample surface. We assume that heat is generated uniformly with power W within the hemisphere. Heat flows outwards from the centre of the hemisphere with spherical symmetry. With a typical collection time, t, of 10 s/pixel, the characteristic thermal diffusion distance, $\sqrt{\kappa t/\rho c_p}$, κ is the thermal conductivity and ρc_p is the volumetric heat capacity is ~4 mm for sapphire, so it is clear that the heat flow occurs at essentially steady state. Outside the generation volume, the total heat energy per unit time crossing any concentric hemispherical surface with radius r must be W at steady state, so:

$$-2\pi r^2 \kappa \frac{dT}{dr} = W \tag{2}$$

where T is the temperature. Inside the sphere:

$$-2\pi r^2 \kappa \frac{dT}{dr} = W \frac{r^3}{r_0^3} \tag{3}$$

These equations can easily be solved subject to the boundary conditions of the far field temperature being attained at large r and temperature continuity at the edge of the generation volume. The maximum temperature increase, ΔT_{max}, occurs at the centre of the hemisphere and is given by:

$$\Delta T_{max} = \frac{3W}{4\pi\kappa r_0}$$

and the volume averaged temperature increase in the generation volume, $\langle \Delta T \rangle$ is given by:

$$\langle \Delta T \rangle = \frac{3W}{5\pi k r_0} \quad .$$

With W=10 kV × 1 nA, $r_0 = 550$ nm and $\kappa = 42$ W m^{-1} K^{-1},[18] $\langle \Delta T \rangle$ is 0.08 °C. Using a temperature dependence of the R_1 line of −0.144 cm^{-1} °C^{-1} and a mean uniaxial piezospectroscopic coefficient of 2.5 cm^{-1} GPa^{-1},[9] the direct effect of temperature on the R_1 wavelength corresponds to an apparent hydrostatic compressive stress of only 4.6 MPa, which is less than the reproducibility of the measurements. There is no simple solution for the actual stress increase in the generation volume caused by the thermal expansion gradient on heating, but an overestimate of the stress level is provided by the case of a spherical volume in the specimen bulk, heated by $\langle \Delta T \rangle$ relative to the material outside it. Use of the Selsing equation[19] shows the resulting compressive stress in the heated volume to be less than 0.3 MPa, which is again negligible.

In conclusion, the excellent agreement between the theoretical and experimental R_1 wavelength shifts around a crack tip, with 550 nm spatial resolution and in the absence of significant specimen heating demonstrates that SEM-CL is a powerful technique for the investigation of near surface stresses in aluminium oxide.

4. Summary

1. Stress-induced shifts in the wavelength of the ruby R-lines in the cathodoluminescence (CL) spectrum excited by the electron beam of an SEM have been mapped around the tip of an indentation crack on the basal plane of a ruby crystal.
2. The shifts agreed well with those expected from the classical crack tip stress field.
3. The stress intensity at the crack tip was 1.0 MPa m$^{1/2}$ which is much less than the toughness of the ruby in fast fracture on the same fracture plane (4.5 MPa m$^{1/2}$). The discrepancy was attributed to slow crack growth and post-indentation lateral cracking.
4. The spatial resolution of the CL measurements at 10 kV was 550 nm which is a factor of 4 better than can be obtained using optical microprobes.
5. The effects of specimen heating were found to be negligible with the conditions used.

References

1. Molis, S. E. and Clarke, D. R., Measurement of stresses using fluorescence in an optical microprobe. *J. Am. Ceram. Soc.*, 1990, **73**, 3189–3194.
2. Belnap, J. D., Tsai, J. F. and Shetty, D. K., Direct measurement of crack shielding in ceramics by the application of Raman microprobe spectroscopy. *J. Mater. Res.*, 1994, **9**, 3183–3193.
3. Siegle, D., Hoffman, A., Eckey, L., Thomsen, C., Bertram, F., Schmidt, D., Rudloff, D. and Hiramatsu, K., Vertical strain and doping gradients in thick GaN layers. *Appl. Phys. Lett.*, 1997, **71**, 2490–2492.
4. Lei, H., Leipner, H. S., Schreiber, J., Weyher, J. L., Wosiński, T. and Grzegory, I., Raman and cathodoluminescence study of dislocations in GaN. *J. Appl. Phys.*, 2002, **92**, 6666–6670.
5. Rudloff, D., Riemann, T., Christen, J., Liu, Q. K. K., Kaschner, A., Hoffman, A., Thomsen, C., Vogeler, K., Diesselberg, M., Einfeld, S. and Hommel, D., Stress analysis of $A_{lx}Ga_{1-x}N$ films with microcracks. *Appl. Phys. Lett.*, 2003, **82**, 367–369.
6. Pezzotti, G., Leto, A., Tanaka, K. and Sbaizero, O., Piezo-spectroscopic assessment of nanoscopic residual stresses in Er^{3+}-doped optical fibres. *J. Phys.: Condens. Matter*, 2003, **15**, 7687–7695.
7. Ostertag, C. P., Robins, L. H. and Cook, L. P., Cathodoluminescence measurement of strained alumina single crystals. *J. Eur. Ceram. Soc.*, 1991, **7**, 109–116.
8. Pezzotti, G., Leto, A., Yamada, K. and Porporati, A. A., Electro-stimulated piezo-spectroscopy for measuring nano-scale residual stress fields in ceramics. *Adv. Sci. Tech.*, 2006, **45**, 1658–1663.
9. He, J. and Clarke, D. R., Determination of the piezospectroscopic coefficients for chromium-doped sapphire. *J. Am. Ceram. Soc.*, 1995, **78**, 1347–1353.
10. Sih, G. C., Paris, P. C. and Irwin, G. R., On cracks in rectilinearly anisotropic bodies. *Int. J. Fract. Mech.*, 1965, **1**, 189–203.
11. Wachtman, J. B., Tefft, W. E., Lam, D. and Stinchfield, R. P., Elastic constants of synthetic single crystal corundum at room temperature. *J. Res. Nat. Bur. Stand.*, 1960, **64A**, 213–228.
12. D. Barnes, High resolution stress measurement in structural ceramics using photo- and cathodo-luminescence, Part II Thesis, University of Oxford 2006.
13. M. Iwasa and T. Ueno, Fracture toughness of quartz and sapphire single crystals at room temperature" Zairyo, vol. 30, no. 337 (1981) 1001-1004.
14. Wiederhorn, S. M., *Mechanical and Thermal Properties of Ceramics*, *303*, ed. J. B. Wachtman Jr. N.B.S. Special Publication, 1969, pp. 217–241.
15. Anstis, G. R., Chantikul, P., Lawn, B. R. and Marshall, D. B., A critical evaluation of indentation techniques for measuring fracture toughness: I, direct crack measurements. *J. Am. Ceram. Soc.*, 1981, **64**, 533–539.
16. Chantikul, P., Anstis, G. R., Lawn, B. R. and Marshall, D. B., A critical evaluation of indentation techniques for measuring fracture toughness: I, strength method. *J. Am. Ceram. Soc.*, 1981, **64**, 539–543.
17. Everhart, T. E. and Hoff, P. H., Determination of kilovolt electron energy dissipation vs penetration distance in solid materials. *J. App. Phys.*, 1971, **42**, 5837–5846.
18. Lee, D. W. and Kingery, W. D., Radiation energy transfer and thermal conductivity of ceramic oxides. *J. Am. Ceram. Soc.*, 1960, **43**, 594–607.
19. Selsing, J., Internal stresses in ceramics. *J. Am. Ceram. Soc.*, 1961, **44**, 419.